A SMALL SCALE PITCH-PLUNGE FLUTTER MODEL FOR ACTIVE FLUTTER CONTROL RESEARCH

A.N. Sutherland
School of Mechanical, Industrial and Aeronautical Engineering
University of the Witwatersrand, Private Bag 3, Johannesburg, 2050, South Africa
ansutherland@gmail.com, Tel.: +27 12 841 3880

Keywords: *Two-dimensional flutter, Airfoil, State-space, Active Control*

ABSTRACT

A pitch-plunge flutter model-mount was designed for active flutter control research. The design is considered novel as it is much smaller and structurally simpler than existing models on which it is based. The mount plunge and pitch stiffnesses and the system mass, mass inertia and centre of gravity can be adjusted, allowing for various test cases. Open-loop test results agreed well with theoretical predictions using classical flutter theory and gentle, low speed flutter was demonstrated. Initial closed-loop simulations using LQG control with a trailing edge flap show that flutter can successfully be suppressed despite the small size of the model and limitations of the actuation servo. The LQG flutter controller, although designed to be optimised for the open-loop flutter speed of the model, suppresses flutter significantly above this speed. For instance, for one simulated test case, flutter was suppressed to 11.1m/s above the predicted open-loop flutter speed of 22.3m/s, a nominal increase of 50%. However, active control wind tunnel testing still has to be done to verify the simulations.

NOMENCLATURE

ab	Distance between mid-chord and elastic axis
$\mathbf{A}$, $\mathbf{B}$, $\mathbf{C}$, $\mathbf{D}$	State-space matrices
b	Airfoil half-chord
c	Non-dimensional distance between airfoil mid-chord and flap hinge line
C	Structural damping
$C(k)$	Theodorsen's function
δ, λ	Coefficients in rational approximation of Wagner function
E	Elastic modulus
f	Frequency in *hz*
G	Shear modulus
I	Area/Mass moment of inertia
$\mathbf{I}$	Identity matrix
J	Torsional stiffness parameter
k	Reduced frequency (Strouhal number)
K	Structural stiffness
ℓ_1, ℓ_2	1st and 2nd Aerodynamic lag state
L	Unsteady lift force, Flexure length
$\mathcal{L}_\delta$, $\mathcal{L}_\lambda$	Matrices of Wagner approximation function coefficients
m	Wing mass
M	Unsteady aerodynamic moment, Structural Mass
N	Number of flexures
Φ	Wagner function
$\mathbf{Q}_1$, $\mathbf{Q}_2$	Matrices of terms proportional to circulation about the airfoil
ρ	Air density
t	Flexure thickness
T	Control surface position function
θ	Flexure angle
u	Control input
U	Free stream velocity
w	Flexure width
ω	Flutter frequency in *rad/s*
x_α	Non-dimensional distance between airfoil pitch axis and airfoil cg
x_β	Non-dimensional distance between flap hinge axis and flap cg

Subscripts:

a	Aerodynamic
α	Pitch
β	Flap angle
c	Command
h	Plunge
s	Structural

1. INTRODUCTION

Airframe structural design trends have shown an increase in flexibility, slenderness ratio and maximum operating speeds which combined can lead to flutter and the potential destruction of the airframe [1]. To increase the flutter boundary of an aircraft without modifying its mass or structural properties and hence limiting its performance, primary flight control surfaces and a feedback control system can be used to actively suppress flutter and stabilise the aircraft above its open-loop flutter speed. As an initial step towards developing and testing such active flutter suppression control laws, two dimensional models representative of a span-wise section of an aircraft wing are often designed and wind tunnel tested. These binary flutter models are an attractive means of experimentally validating active flutter control laws because of their gentle, low speed and well defined flutter characteristics. In view of this, a small-scale pitch-plunge flutter model was designed for active flutter control research to be done in the University of the Witwatersrand's low speed continuous wind tunnel [2]. The model had to be small in size to suit the small elliptical test section of the wind tunnel and to minimise cost. It was also required that the model have a low flutter speed and gentle flutter characteristics.

2. THEORY

2.1. Pitch-Plunge Flutter

Simplified two-dimensional aerodynamic theory adequately models the unsteady aerodynamic forces and moments acting on an airfoil with pitch, plunge and control surface degrees of freedom. Various two-dimensional methods have been developed to calculate these forces and moments [3]. Theodorsen's method [4] was used in this study. This theory is limited to airfoils with thin sections of infinite span undergoing small oscillations in all vibration modes. Flow over the airfoil is assumed to remain potential and un-separated and the structural equations of the system are linearised [5]. The airfoil pitches about its elastic axis. It is assumed the control surface is aerodynamically balanced and pivots about its leading edge [4]. Figure 2.1 shows a schematic of such an airfoil and control surface. The elastic axis and airfoil centre of mass positions are measured positive aft of the airfoil mid-chord.

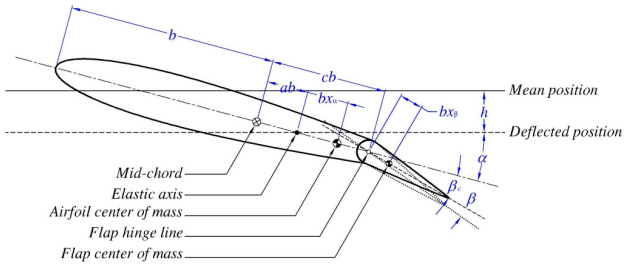

Figure 2.1 Flutter Model Notations

The forces acting on the airfoil are the unsteady lift L (assumed to act at the quarter chord position), unsteady pitching moment M_α and unsteady flap hinge moment M_β as shown in Figure 2.2. Using Lagrange's method, the linearised equations of motion of the system depicted in Figure 2.2 are [4]:

$$m\ddot{h} + mx_\alpha b\ddot{\alpha} + mx_\beta b\ddot{\beta} + C_h h + K_h h = L \quad \text{.....(2.1)}$$

$$mx_\alpha b\ddot{h} + I_\alpha \ddot{\alpha} + \left[(c-a)b^2 mx_\beta + I_\beta\right]\ddot{\beta} + C_\alpha \dot{\alpha} + K_\alpha \alpha = M_\alpha \quad \text{.....(2.2)}$$

$$mx_\beta b\ddot{h} + \left[(c-a)b^2 mx_\beta + I_\beta\right]\ddot{\alpha} + I_\beta \ddot{\beta} + C_\beta \dot{\beta} + K_\beta(\beta - \beta_c) = M_\beta \quad \text{.....(2.3)}$$

The unsteady lift, pitching moment and flap hinge moment are described in terms of the instantaneous configuration of the system (position, rate and acceleration of all vibration modes). L, M_α and M_β per unit wingspan are then given as [3]:

$$L = -\rho b^2\left(\pi\ddot{h} - \pi ba\ddot{\alpha} - bT_1\ddot{\beta} + U\pi\dot{\alpha} - UT_4\dot{\beta}\right) - 2\pi\rho bC(k)\left[\dot{h} + b\left(\tfrac{1}{2} - a\right)\dot{\alpha} + \tfrac{1}{2\pi}bT_{11}\dot{\beta} + U\alpha + \tfrac{1}{\pi}T_{10}U\beta\right] \quad \text{.....(2.4)}$$

$$M_\alpha = -\rho b^2\left\{-\pi ab\ddot{h} + \pi b^2\left(\tfrac{1}{8}+a^2\right)\ddot{\alpha} - b^2\left[T_7 + (c-a)T_1\right]\ddot{\beta} + \right.$$
$$\pi bU\left(\tfrac{1}{2}-a\right)\dot{\alpha} + bU\left[T_1 - T_8 - (c-a)T_4 + \tfrac{1}{2}T_{11}\right]\dot{\beta} + (T_4 + T_{10})U^2\beta\Big\} - \quad \text{.....(2.5)}$$
$$2\pi\rho b^2 U\left(\tfrac{1}{2}+a\right)C(k)\left[\dot{h} + b\left(\tfrac{1}{2}-a\right)\dot{\alpha} + \tfrac{1}{2\pi}bT_{11}\dot{\beta} + U\alpha + \tfrac{1}{\pi}T_{10}U\beta\right]$$
$$M_\beta = -\rho b^2\left\{-bT_1\ddot{h} + 2b^2T_{13}\ddot{\alpha} - \tfrac{1}{\pi}b^2T_3\ddot{\beta} - Ub\left[2T_9 + T_1 - T_4\left(\tfrac{1}{2}-a\right)\right]\dot{\alpha} - \right.$$
$$\tfrac{1}{2\pi}UbT_4T_{11}\dot{\beta} + \tfrac{1}{\pi}U^2\left(T_5 - T_4T_{10}\right)\beta\Big\} - \rho b^2UT_{12}C(k)\left[\dot{h} + b\left(\tfrac{1}{2}-a\right)\dot{\alpha} + \quad \text{.....(2.6)}$$
$$\tfrac{1}{2\pi}bT_{11}\dot{\beta} + U\alpha + \tfrac{1}{\pi}T_{10}U\beta\right]$$

where the 'T' terms are a function of the flap position and can be found in [4]. *C(k)* accounts for lift due to vortices being shed off the trailing edge of the wing because of its motion, and is expressed in terms of Bessel (or Hankel) functions.

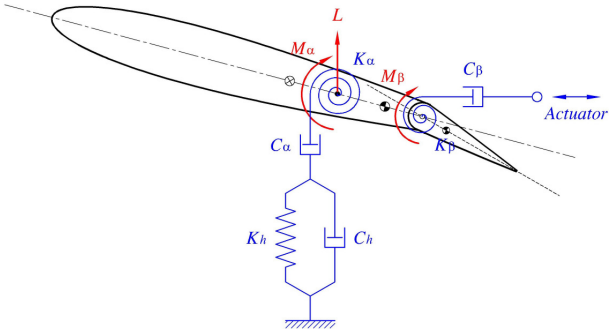

Figure 2.2 Schematic of Flutter Model

Some models (see [6], [7] for example) omit the effect that these shed vortices (wake circulation) have on the flutter speed, and are termed *quasi-steady* solutions. However, in this work the aerodynamic lag effects have been included. To model these effects, a rational approximation to Theodorsen's function is needed. To get this, Wagner's function, which is the inverse Fourier transform of Theodorsen's function divided by $i\omega$, as shown in Equation (2.7), is approximated by the two-term function given in Equation (2.8) [8]:

$$\Phi = \mathcal{F}^{-1}\left\{\frac{C(k)}{i\omega}\right\} \quad \text{.....(2.7)}$$

$$\Phi = 1 - \delta_1 e^{\frac{-\lambda_1 Ut}{b}} - \delta_2 e^{\frac{-\lambda_2 Ut}{b}} \quad \text{.....(2.8)}$$

In Equation (2.8) δ_1 = 0.165, λ_1 = 0.041, δ_2 = 0.335 and λ_2 = 0.320 as given in [8]. Equations (2.1), (2.2) and (2.3) (structural equations of the system) are combined with Equations (2.4), (2.5) and (2.6) (generalised aerodynamic forces) to form the equations of motion of the system. Equation (2.8) is used to approximate the circulatory lift contribution to the unsteady aerodynamic forces. The combined equations (not shown) are written in a *state-space* form for subsequent addition of a control input to suppress flutter, as described briefly in §2.2 below.

2.2. Active Flutter Control

Using time domain control theory the state-space equations of motion of the dynamic system are [9]:

$$\left.\begin{aligned}\dot{\mathbf{X}} &= \mathbf{A}\mathbf{X} + \mathbf{B}u\\ \mathbf{Y} &= \mathbf{C}\mathbf{X} + \mathbf{D}u\end{aligned}\right\} \quad \text{.....(2.9)}$$

where $u = \beta_c$ is the commanded flap angle. $\mathbf{A}, \mathbf{B}, \mathbf{C}, \mathbf{D}$ are given in Appendix A. The system consists of eight states viz. the plunge deflection, pitch angle, flap angle, their respective rates and two aerodynamic lag states, since a two-term approximation to the Wagner function is used. In vector notation:

$$\mathbf{X} = \left[\dot{h} \quad \dot{\alpha} \quad \dot{\beta} \quad h \quad \alpha \quad \beta \quad \ell_1 \quad \ell_2\right]^T \quad \text{.....(2.10)}$$

The initial simulations assume that pitch rate, plunge rate and flap angle are measured and the remaining five states are estimated. Linear Quadratic Regulator (LQR) control is used to calculate feedback gains and a Kalman filter is used to estimate unmeasured states. An example of results obtained from initial simulations, using this Linear Quadratic Gaussian (LQG) controller is given in §4.2.

3. MODEL DESIGN

3.1. Model Mount

Two common pitch-plunge flutter model design approaches are reported in the literature. One approach employs flexures, whilst the second uses coil springs to achieve desired pitch and plunge modal frequencies.

Farmer [10] describes the design of a large pitch-plunge flutter model in which a rigid wing is attached to a splitter plate mounted on four circular rods and a central horizontal rectangular drag strut, all cantilevered from the sidewall of a wind tunnel. A cross-section through this mount is shown in Figure 3.1.

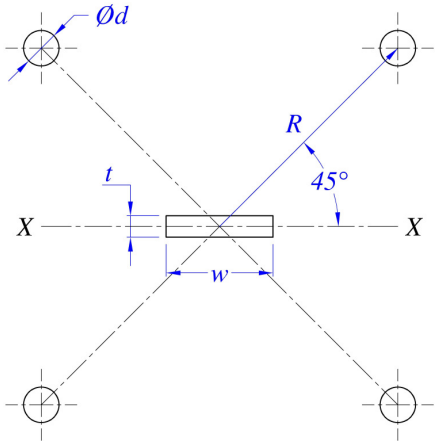

Figure 3.1 Flexure Pitch-Plunge Mount [10]

The function of the drag strut is to make the in-plane stiffness of the mount significantly higher than its transverse stiffness, whilst contributing minimally to its torsional stiffness. The rods are fixed and constrained by plates at either end, so the deflection slopes there are zero as the splitter plate moves, resulting in simple pitch-plunge movement. Another advantage of flexure constrained flutter models is that structural damping is very low (can be considered negligible) and remains constant as loads on the model vary. Thus aerodynamic damping is essentially the only damping influencing the motion of the wing. This enables investigation of changes in aerodynamic damping with air flow over the wing [10]. Dansberry *et al* [11] improved Farmer's mount [10] by reducing the size of the splitter plate and using it only as a means to mount the flexures to the wing. A second splitter plate, un-connected to the model, was used to separate the airflow over the model and the mount. The advantage of this system is that mechanical stops can be mounted on the second splitter plate to arrest flutter should the amplitude of the oscillation grow too large.

The alternative approach to the design of a pitch-plunge flutter model, using an arrangement of coil springs to constrain the motion of a rigid wing, is described in [12], [13]. This system allows pitch and plunge stiffnesses to be varied *independently* and can be used to investigate the effect of a non-linear restoring force on the flutter characteristics of a rigid wing [12]. The main disadvantages of the spring system are the introduction of significant structural damping into the flutter model and the relatively high cost [12].

In this work [2] a new design was developed based on [10], but using *rectangular* flexures. This eliminated the need for the central drag strut and made the small-size mount feasible. A cross-section through the new mount design is shown in Figure 3.2. This design is thought to be novel as no similar implementation could be found in the literature. An interesting feature of this design is that the flexures can be rotated to a position where pitch, plunge and in-plane bending frequencies will occur in a similar range. Inclusion of the additional degree of freedom (in-plane bending) could be a topic for future research.

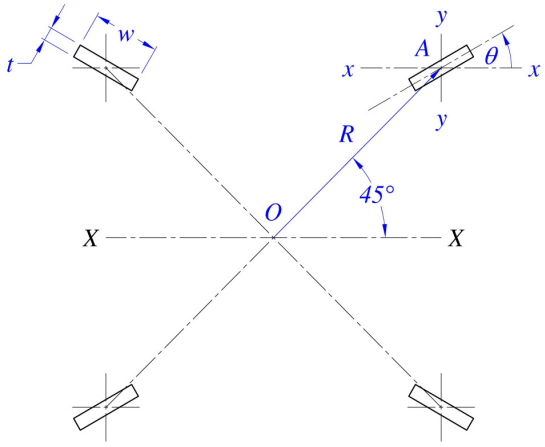

Figure 3.2 New Flexure Mount [2]

The stiffness of the plunge degree of freedom of the mount is given by Equation (3.1) and that of the pitch degree of freedom by Equation (3.2), taken from [14]:

$$K_h = \frac{12EI_{xx}}{L^3} \quad \text{.....(3.1)}$$

$$K_\alpha = N\frac{GJ}{L} + \frac{12EI_{OA}}{L^3} \quad \text{.....(3.2)}$$

The torsional stiffness parameter J in Equation (3.2) is given by [14]:

$$J = wt^3\left(\frac{1}{3} - 0.21\left(\frac{t}{w}\right)\left[1 - \frac{1}{12}\left(\frac{t}{w}\right)^4\right]\right) \quad \text{.....(3.3)}$$

and the area moments I_{xx}, I_{yy} and I_{OA} by [14]:

$$I_{xx} = \frac{wt}{12}\left[(w\sin\theta)^2 + (t\cos\theta)^2\right] \quad \text{.....(3.4)}$$

$$I_{yy} = \frac{wt}{12}\left\{\left[w\sin(90^\circ - \theta)\right]^2 + \left[t\cos(90^\circ - \theta)\right]^2\right\} \quad \text{.....(3.5)}$$

$$I_{OA} = \frac{wt}{12}\left\{\left[w\sin(45^\circ - \theta)\right]^2 + \left[t\cos(45^\circ - \theta)\right]^2\right\} \quad \text{.....(3.6)}$$

Pitch and plunge frequencies of the mount are then given by Equations (3.7) and (3.8), as in [10]:

$$f_h = \frac{1}{2\pi}\sqrt{\frac{K_h}{m}} \quad \text{.....(3.7)}$$

$$f_\alpha = \frac{1}{2\pi}\sqrt{\frac{K_\alpha}{I_\alpha}} \quad \text{.....(3.8)}$$

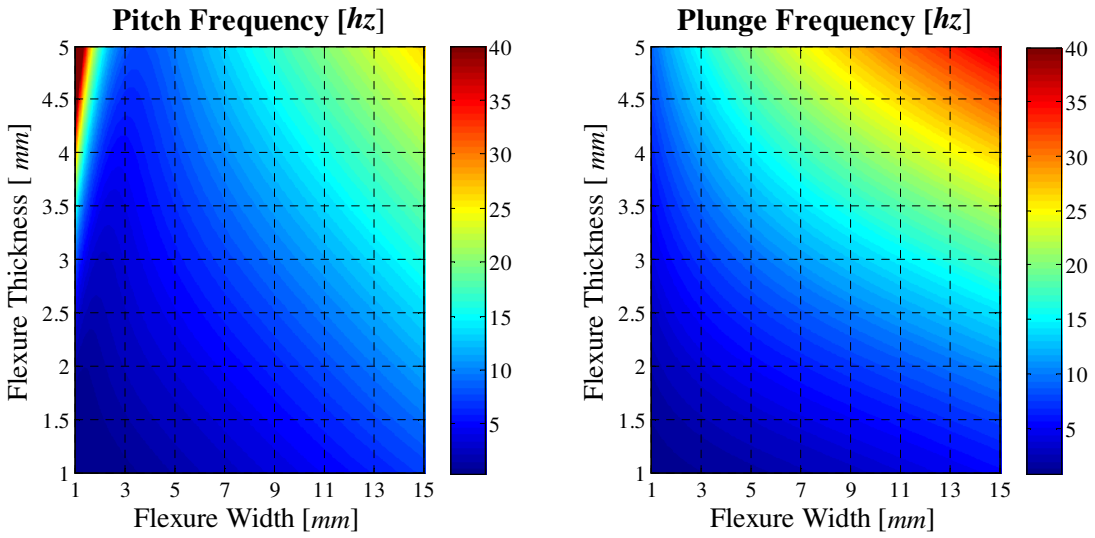

Figure 3.3 Effect of Flexure Width and Thickness on Pitch and Plunge Frequencies

Using AISI-01 tool steel for the flexures, and for a given wing mass and mass inertia, parametric studies were done to establish the effect of w, t, L, θ, R and N on the structural properties of the model, hence its flutter characteristics. A sample parametric contour plot is shown in Figure 3.3 (for N = 4). This analysis enabled a flutter model to be designed that was suitable for testing within the geometric and operational constraints of the University of the Witwatersrand's low speed wind tunnel. For a fixed elastic axis position the pitch and plunge stiffnesses can be varied by changing the orientation θ of the flexures. The model was designed to allow each flexure to be aligned at four different, fixed angles, locked in place with a steel dowel pin. A simple fairing was fitted ahead of the flexures so that they did not generate any aerodynamic forces themselves which would change the flutter characteristics of the wing. A rigid wing comprising an aluminium framework and balsa wood inserts, with a chord of 120*mm*, span of 360*mm* and a NACA0012 profile was attached to the mount. Model mass, mass inertia and centre of gravity were varied independently using sliding ballast masses. Two CTC-AC140-1A accelerometers located at the wing root were used to measure

the dynamic response of the wing. Mechanical stops were incorporated in the model mount to prevent excessive motion, and hence damage, as flutter was encountered. The complete model, as mounted in the University of the Witwatersrand's wind tunnel, is shown in Figure 3.4.

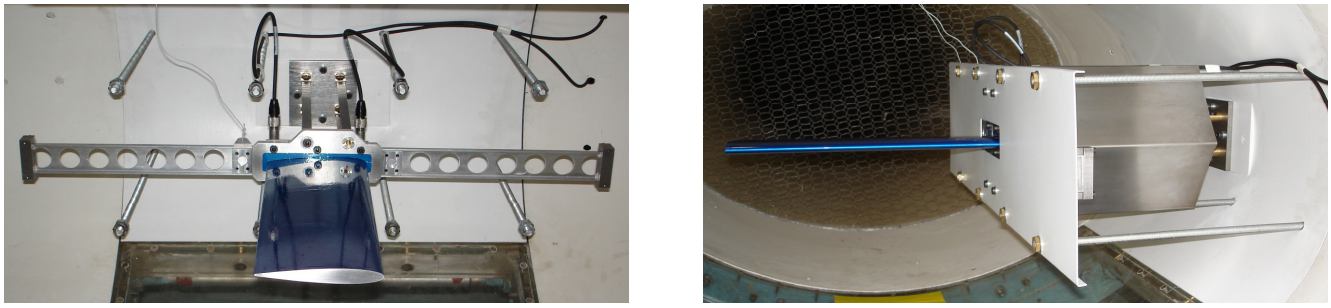

(a) Splitter Plate and Fairing Removed

(b) Complete Model-Mount as Tested

Figure 3.4 Flutter Model Mounted in the University of the Witwatersrand's Low Speed Continuous Wind Tunnel

3.2. Active Control Wing

A second wing model incorporating a trailing edge flap was designed for active flutter control research with the existing flexible mount. This model is shown in Figure 3.5. The additional control surface degree of freedom will be actively controlled to suppress flutter. The internal structure of the wing comprises aluminium and carbon fibre ribs and carbon fibre spars. A carbon fibre skin slides over the whole framework and is pinned in several places to the ribs, to provide additional stiffness and the aerodynamic shape. A novel feature of this active control wing is that the flap is controlled through a torsion flexure, designed to ensure the flap rotation frequency is higher than the pitch and plunge frequencies of the wing. The actuator used to drive the flap is a Hitec® HS-5125MG model aircraft servo.

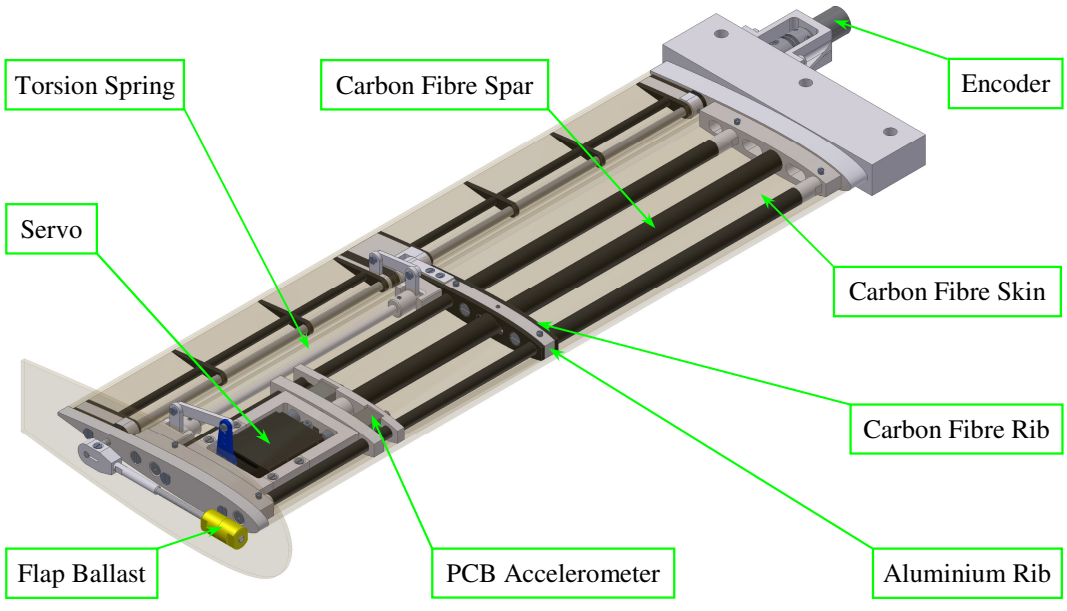

Figure 3.5 Active Control Wing

This servo was selected because of its small size, relatively high speed and good torque characteristics. The servo is a digital type, requiring only a single pulse width modulated (PWM) signal for actuation. Because of this, it has a smaller dead-band and better position resolution than similar analogue servos. A Contelec Vert-X 13 contactless encoder, located at the wing root, is used to measure flap angle. Two PCB type 333B32 accelerometers, located inside the wing, are used to measure its dynamic response. A National Instruments NI USB-6211 multifunction data acquisition (DAQ) card is used to acquire data and control the servo. The DAQ card is controlled by software written in C# and Matlab® (using the data acquisition toolbox) via a computer in the loop.

4. RESULTS

4.1. Open-Loop Results

Open-loop flutter testing was carried out in the University of the Witwatersrand's low speed continuous wind tunnel, with θ = 2.5º, 3.5º and 4.5º. The configuration with θ = 5.5º was not tested because of limited time[1] and wind tunnel schedule. For each configuration, testing began at wind speeds much lower than the predicted flutter speed. As the model has no in-built excitation, and tunnel turbulence is low, the model was excited by giving it an initial displacement and then allowing it to oscillate

Table 4.1 Open-Loop Model Parameters

Parameter	*Units*	*Value*
a	/	-0.20
b	m	0.06
m	kg	1.58
I_α	kgm^2	0.0355
f_α	hz	6.66
f_h	hz	6.02
Wingspan	m	0.35
ρ	kg/m^3	1.0062

[1] 8 weeks to complete the research and submit the final dissertation, including design & manufacture of the model.

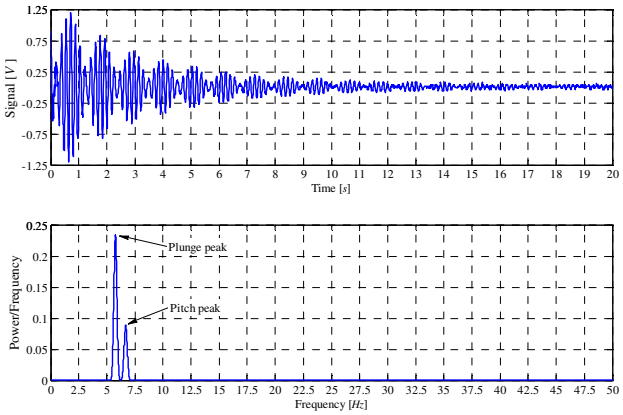

Figure 4.1 Wind off Time Series

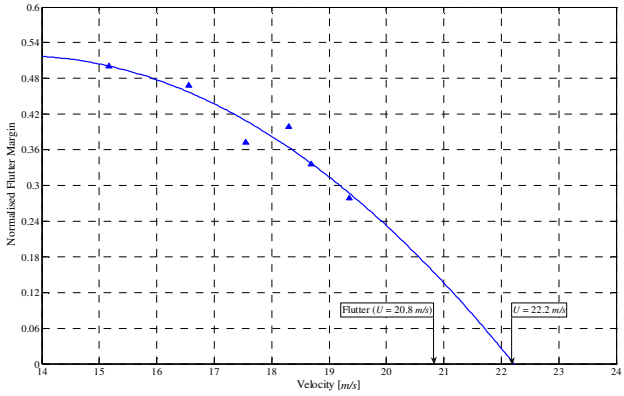

Figure 4.2 Simplified Zimmerman Flutter Margins

freely whilst recording the data. Recorded data was read into Matlab® and smoothed with a standard smoothing algorithm. A Hamming window function [15] was applied to the smoothed data and a Fast Fourier Transform (FFT) performed to establish the modal frequencies (Figure 4.1). Once the pitch and plunge frequencies of the model had been established, the simplified Zimmerman flutter-margin criterion [16] was used to calculate the flutter margin of the model for the given wind tunnel speed. The wind tunnel speed was then increased, and the above process repeated, whilst the simplified Zimmerman flutter margin was tracked to predict the onset of flutter (Figure 4.2). Testing of the first two configurations (θ = 2.5º, 3.5º) was intentionally stopped before their respective flutter speeds were reached, to allow the structural and aerodynamic properties of the mount to be accurately characterised. The model was then

allowed to flutter in the third configuration (θ = 4.5º). This was achieved by slowly approaching flutter, based on a flutter speed predicted by extrapolating a curve fit of calculated Zimmerman flutter margins from the lower test speeds (Figure 4.2). Gentle, low speed flutter was demonstrated and the model behaved as anticipated. Test results were in excellent agreement with the prediction. With the flexures set to θ = 4.5º the still air plunge frequency was 6.02hz and the pitch frequency 6.66hz (Figure 4.1). Flutter occurred at 6.36hz at a speed of 20.79m/s, compared with the theoretical prediction of 6.54hz at a speed of 20.81m/s. A single flutter cycle, photographed during this test, is shown in Figure 4.3. This flutter was demonstrated repeatedly and consistently without damage to the model.

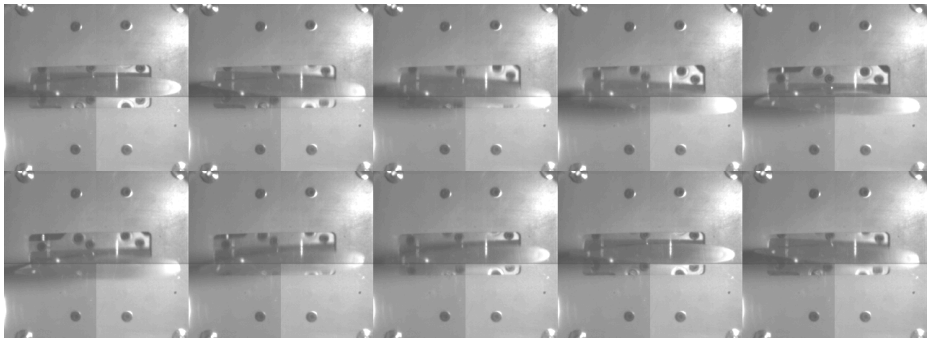

Figure 4.3 Single Flutter Cycle at 6.36Hz

4.2. Closed Loop Simulations

Initial simulations using LQR control and a Kalman filter (i.e. LQG control) indicate that despite the small scale of the model and limitations of the servo used to actuate the flap, flutter can be suppressed to a good margin above the open-loop flutter speed. Two approaches were used to investigate the effectiveness of the flutter controller. The first approach used a state-space model of the complete system, and was developed in Matlab®. The second approach used a Simulink® model. Both simulations gave the same result, but the Simulink® model is preferable since the control input (flap angle) can be position and rate limited, and dead-band easily added, to better model the flap actuator (servo). The natural frequencies of the mount were calculated from Equations (3.7) and (3.8). The mass and mass inertia of the new wing were estimated from CAD drawings of the model after assigning material properties to each component. For an anticipated wing mass of 1.80kg, mass inertia of 0.0382kgm^2 and other parameters similar to those listed in Table 4.1, open-loop flutter was predicted to occur at 22.28m/s. A flap hinged at 75% of the wing chord, controlled with a flutter controller optimised for the predicted open-loop flutter speed, effectively suppresses flutter up to a velocity of 33.42m/s, a nominal increase of 50% in the flutter speed of the model. Figure 4.4 shows the closed-loop control of predicted and Kalman estimated pitch, plunge and flap angle states at the open-loop flutter speed. It is apparent that the flutter controller is able to suppress flutter within 5.0s. At the time of writing, wind tunnel tests still have to be performed to verify these predictions.

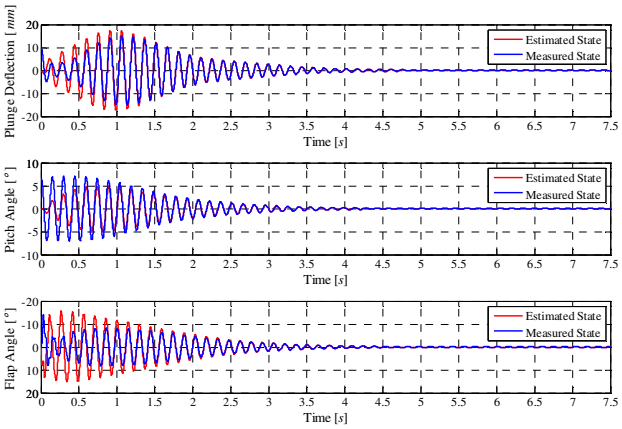

Figure 4.4 Closed-Loop Simulation

5. CONCLUSIONS

A novel small-scale, low cost pitch-plunge flutter model was successfully designed and wind tunnel tested. The model is capable of exhibiting classical pitch-plunge flutter without sustaining damage. Experimental results agree well with predictions from classical flutter theory. Due to the success of the initial phase of this project, work has proceeded on the addition of a control surface (trailing edge flap) and digital control system for research into active flutter control. Initial closed-loop simulations using Matlab® and Simulink® predict that flutter can be suppressed adequately using LQR control and a Kalman filter, despite the small size of the model and limitations of the servo. Given the small scale and low cost of the model, it is an ideal testbed for research into active flutter control, in particular to quickly test and verify different control algorithms. At the time of writing, closed-loop wind tunnel tests still have to be done.

6. ACKNOWLEDGEMENTS

Thanks go to Dr. Craig Law[2] for supervising this project, to Mr. Andrew Sutherland and Mr. Louw van Zyl[3] for their advice and interest in this work and to the CSIR, The University of the Witwatersrand and National Aerospace Centre of Excellence (NACoE) for their generous funding of the project.

7. REFERENCES

[1] Thompson, G.O. and Kass, G.J. 1971. Active flutter suppression - an emerging technology, *Journal of Aircraft*. Vol. 9, No. 3. pp. 230 - 235.

[2] Sutherland, A.N. 2006. The aeroelastic response of a rigid wing: a pitch-plunge flutter investigation. BSc. (Eng.) Report. University of the Witwatersrand. Johannesburg.

[3] Scanlan, R.H. and Rosenbaum, R. 1968. *Introduction to the study of aircraft vibration and flutter*. Dover Publications, Inc. New York.

[4] Theodorsen, T. 1949. General theory of aerodynamic instability and the mechanism of flutter, NACA-TR-496. National Advisory Commission for Aeronautics.

[5] Fung, Y.C., 1955. *An introduction to the theory of aeroelasticity*. John Wiley and Sons, Inc., New York.

[6] Dowell, E.H.*et al*. 1995. *A modern course in aeroelasticity*, 3rd Revised and Enlarged Edition. Kluwer Academic Publishers.

[7] Ursu, I. et al. 2004. Active control laws for flutter suppression. Annals of University of Craiova, No. 27.

[8] Rodden, W.P. and Stahl, B. 1969. A strip method for prediction of damping in subsonic wind tunnel and flight flutter tests. *Journal of Aircraft*. Vol. 6, No. 1. pp. 9 - 17.

[9] Franklin, G.F *et al*. 1991. *Feedback control of dynamic systems*. Addison-Wesley Publishing Company.

[10] Farmer, M.G. 1982. A two-degree of freedom mount system with low damping for testing rigid wings at different angles of attack, NASA-TM-83302. Langley Research Center.

[11] Dansberry, B.E. *et al*. 1993. Physical properties of the benchmark models program supercritical wing. NASA-TM-4457. NASA.

[12] O'Neil, T and Strganac, T.W. 1998. Aeroelastic response of an airfoil supported by nonlinear springs. *Journal of Aircraft*. Vol. 35, No. 4. pp. 616 - 622.

[13] Gan Chowdhury, A and Sarkar, P.P. 2003. A new technique for identification of eighteen flutter derivatives using a three-degree-of-freedom Section Model. *Engineering Structures*, Vol. 25, No. 14. pp. 1763 - 1772.

[14] Roark, R.J. and Young, W.C. 1975. *Formulas for stress and strain, 5th Ed*. McGraw-Hill.

[15] Otnes, R.K. & Enochson, L. 1978. *Applied time series analysis, Volume 1: Basic techniques*. John Wiley and Sons. New York

[16] Zimmerman, N.H. and Weissenburger, J.T. 1964. Prediction of flutter onset speed based on flight testing at subcritical speeds. *J. Aircraft*, Vol. 1, No.4, pp. 190-202.

COPYRIGHT STATEMENT

[2] University of the Witwatersrand.
[3] CSIR.

APPENDIX A

The state-space matrices given in §2.2 are listed below for convenience. The system matrix of the 3DOF flutter system is:

$$\mathbf{A} = \left[\begin{array}{c|c|c} -\bar{\mathbf{M}}^{-1}\bar{\mathbf{C}} & -\bar{\mathbf{M}}^{-1}\bar{\mathbf{K}} & -\bar{\mathbf{M}}^{-1}\mathcal{L}_{\delta} \\ \hline \mathbf{I}_{3\times 3} & \mathbf{0}_{3\times 3} & \mathbf{0}_{3\times 2} \\ \hline -\mathbf{Q}_1\bar{\mathbf{M}}^{-1}\bar{\mathbf{C}}+\mathbf{Q}_2 & -\mathbf{Q}_1\bar{\mathbf{M}}^{-1}\bar{\mathbf{K}} & -\mathbf{Q}_1\bar{\mathbf{M}}^{-1}\mathcal{L}_{\delta}+\mathcal{L}_{\lambda} \\ -\mathbf{Q}_1\bar{\mathbf{M}}^{-1}\bar{\mathbf{C}}+\mathbf{Q}_2 & -\mathbf{Q}_1\bar{\mathbf{M}}^{-1}\bar{\mathbf{K}} & -\mathbf{Q}_1\bar{\mathbf{M}}^{-1}\mathcal{L}_{\delta} \end{array}\right] \quad \text{(A1)}$$

and the input matrix is:

$$\mathbf{B} = \begin{bmatrix} -\bar{\mathbf{M}}^{-1}K_{\beta} \\ \mathbf{0}_{5\times 1} \end{bmatrix} \quad \text{(A2)}$$

The measurement matrix is:

$$\mathbf{C} = \begin{bmatrix} 1 & 0 & 0 & 0 & 0 & 0 & 0 & 0 \\ 0 & 1 & 0 & 0 & 0 & 0 & 0 & 0 \\ 0 & 0 & 0 & 0 & 0 & 1 & 0 & 0 \end{bmatrix} \quad \text{(A3)}$$

and the feed-through matrix is:

$$\mathbf{D} = \mathbf{0}_{3\times 1} \quad \text{(A4)}$$

since no feed-forward control is used. The mass, damping and stiffness matrices given in Equation (A1) are:

$$\left.\begin{aligned} \bar{\mathbf{M}} &= \mathbf{M}_s - \mathbf{M}_a \\ \bar{\mathbf{C}} &= \mathbf{C}_s - \mathbf{C}_a \\ \bar{\mathbf{K}} &= \mathbf{K}_s - \mathbf{K}_a \end{aligned}\right\} \quad \text{(A5)}$$

The structural matrices in Equation (A5) are:

$$\mathbf{M}_s = \begin{bmatrix} m & mx_{\alpha}b & mx_{\beta}b \\ mx_{\alpha}b & I_{\alpha} & (c-a)b^2mx_{\beta}+I_{\beta} \\ mx_{\beta}b & (c-a)b^2mx_{\beta}+I_{\beta} & I_{\beta} \end{bmatrix} \quad \text{(A6)}$$

$$\mathbf{C}_s = \begin{bmatrix} C_h & 0 & 0 \\ 0 & C_{\alpha} & 0 \\ 0 & 0 & C_{\beta} \end{bmatrix} \quad \text{(A7)}$$

$$\mathbf{K}_s = \begin{bmatrix} K_h & 0 & 0 \\ 0 & K_{\alpha} & 0 \\ 0 & 0 & K_{\beta} \end{bmatrix} \quad \text{(A8)}$$

and the "aerodynamic" matrices in Equation (A5) are[4]:

$$\mathbf{M}_a = \rho b^3 \begin{bmatrix} -\frac{\pi}{b} & \pi a & T_1 \\ \pi a & -\pi b\left(\frac{1}{8}+a^2\right) & b\left[T_7+(c-a)T_1\right] \\ T_1 & -2bT_{13} & \frac{1}{\pi}bT_3 \end{bmatrix} \quad \text{(A9)}$$

$$\mathbf{C}_a = \rho b^2 U \begin{bmatrix} -\frac{2\pi}{b} & -2\pi(1-a) & T_4-T_{11} \\ 2\pi\left(\frac{1}{2}+a\right) & 2\pi ba\left(\frac{1}{2}-a\right) & b\left[T_8-T_1+(c-a)T_4+aT_{11}\right] \\ -T_{12} & b\left[2T_9+T_1+(T_4-T_{12})\left(\frac{1}{2}-a\right)\right] & \frac{1}{2\pi}bT_{11}(T_4-T_{12}) \end{bmatrix} \quad \text{(A10)}$$

$$\mathbf{K}_a = \rho b^2 U^2 \begin{bmatrix} 0 & -\frac{2\pi}{b} & -\frac{2T_{10}}{b} \\ 0 & 2\pi\left(\frac{1}{2}+a\right) & 2aT_{10}-T_4 \\ 0 & -T_{12} & -\frac{1}{\pi}\left[T_5-T_{10}(T_4-T_{12})\right] \end{bmatrix} \quad \text{(A11)}$$

The matrices in Equation (A1) that account for aerodynamic lag are:

$$\mathbf{Q}_1 = \begin{bmatrix} 1 & b\left(\frac{1}{2}-a\right) & \frac{1}{2\pi}bT_{11} \end{bmatrix} \quad \text{(A12)}$$

$$\mathbf{Q}_2 = \begin{bmatrix} 0 & U & \frac{1}{\pi}T_{10} \end{bmatrix} \quad \text{(A13)}$$

$$\mathcal{L}_\delta = \rho b^2 U \begin{bmatrix} \frac{2\pi\delta_1}{b} & \frac{2\pi\delta_2}{b} \\ -2\pi\left(\frac{1}{2}+a\right)\delta_1 & -2\pi\left(\frac{1}{2}+a\right)\delta_2 \\ T_{12}\delta_1 & T_{12}\delta_2 \end{bmatrix} \quad \text{(A14)}$$

$$\mathcal{L}_\lambda = \begin{bmatrix} -\frac{\lambda_1 U}{b} & 0 \\ 0 & -\frac{\lambda_2 U}{b} \end{bmatrix} \quad \text{(A15)}$$

[4] It is shown in [4] that $T_{13} = -\frac{1}{2}\left[T_7+(c-a)T_1\right]$, thus the aerodynamic mass matrix is symmetric as required.